INTERNATIONAL JOURNAL FOR NUMERICAL AND ANALYTICAL METHODS IN GEOMECHANICS
Int. J. Numer. Anal. Meth. Geomech., **22**, 1001–1020 (1998)

ANALYSIS OF STONE-COLUMN REINFORCED FOUNDATIONS

J. S. LEE*,† AND G. N. PANDE‡

Department of Civil Engineering, University of Wales Swansea, SA2 8PP, U.K.

SUMMARY

A numerical model is proposed to analyse elastic as well as elastoplastic behaviour of stone-column reinforced foundations. The stone-columns are assumed to be dispersed within the *in situ* soil and a homogenization technique is invoked to establish equivalent material properties for *in situ* soil and stone-column composite. The difficulties encountered in carrying out elastoplastic analyses of composite materials are overcome by adopting a separate yield function for each of the constituent materials and a sub-iteration procedure within an implicit backward Euler stress integration scheme. In the proposed procedure, equilibrium as well as kinematic conditions implied in the homogenization procedure are satisfied for both elastic as well as elastoplastic stress states.

The proposed model is implemented in an axi-symmetric finite element code and numerical prediction is made for the behaviour of model circular footings resting on stone-column reinforced foundations. This prediction indicates good agreement with experimental observation. Finally, a new scheme in which the length of stone-column is variable is proposed and its behaviour is examined through a numerical example.

Key words: stone-column reinforcement; homogenisation technique; elastoplastic analysis; sub-iteration scheme

1. INTRODUCTION

Stone-columns are extensively used to improve bearing capacity of poor ground and reduce settlements of structures built on them. Their analysis and design is carried out according to simplified rules of thumb which are largely based on the results of model and *in situ* tests on single stone-columns and past experience. The main aim of this paper is to provide a basis for a rational method of analysis and design of stone-column reinforced foundations.

The construction of stone-columns is generally carried out using either a *replacement* or a *displacement* method. In the replacement or wet method, native soil is replaced by stone-columns in a regular pattern where the holes are constructed using a vibratory probe (vibroflot) accompanied by a water jet. As can be expected, this method is suitable where ground water level is high and *in situ* soil is relatively soft. In the displacement or dry method, native soil is displaced laterally by a vibratory probe using compressed air. This installation method is appropriate

† Korea Highspeed Rail Construction, Formerly Research Student
‡ Professor

*Correspondence to: J. S. Lee, Email: mikelee@chollian.net

CCC 0363–9061/98/121001–20$17.50

Received 1 March 1996
Revised 30 January 1998

where ground water level is low and *in situ* soil is firm. Other installation methods, e.g. dynamic ramming or sand compaction, have also been used to construct stone-columns, see Munfakh *et al.*,[1] but are less common in practice.

A rigorous analysis of stone-column reinforced foundation is difficult since three-dimensional behaviour of the ground involving stone-columns has to be considered to get a realistic solution. In the past, the following approximate solutions have been proposed:

(a) *Unit cell approximation*: Attempts to analyse the stone-column reinforced foundation have been made by representing reinforced ground by a unit *cell* with the stone-column at the centre. This approximation gives a reasonable result if the influence of the boundary conditions is negligible, e.g., References 2–5. Balaam and Booker have derived elastic[6] and elastoplastic[7] solutions for the unit cell subject to uniform vertical displacement. Applying confining pressure along the outer boundary, a solution which violates the continuity (or equilibrium) condition in the radial direction is first obtained. Next, the equilibrium condition is satisfied by applying redundant radial stress on the stone-column and the surrounding clay in opposite directions. The final solution is the superposition of these two solutions. When the column is modelled as an elastic-perfectly plastic material obeying Mohr–Coulomb yield criterion, the solution is obtained through imposing the continuity conditions both for stress as well as displacement in the radial and vertical directions, respectively. The unit cell approximation has the disadvantage that it can only be used where the influence of the boundary conditions can be neglected and where loads are applied parallel to the vertical direction. However, if the material properties under consideration are not uniform, or if non-linearity of the *in situ* soil has to be accounted for, the above-mentioned unit cell method may not be appropriate. Here, a homogenisation technique, discussed below, together with finite element method can be introduced.

(b) *Homogenization techniques*: In this approach, stone-column reinforced soil is treated as a composite material. Once adequate stress–strain response of the composite is defined, the response of stone-column reinforced foundation subject to arbitrary loadings and boundary conditions can be studied. The first attempt to solve the reinforced ground employing a homogenization technique on a purely numerical basis was made by Mitchell and Huber.[8] In this, using axi-symmetric characteristics of the stone-column reinforcement instead of fully three-dimensional geometry, all columns are homogenized and replaced by cylindrical rings with the same area ratio. A more realistic approach with the homogenization technique has been proposed by Schweiger[9] and Schweiger and Pande[10,11] by employing modified Voigt assumptions. Since Voigt assumptions in the radial direction lead to the violation of the equilibrium conditions, a pseudo-yield criterion is proposed such that radial equilibrium condition is satisfied. Both *in situ* soil and stone-column materials may have elastoplastic characteristics in the formulations and a viscoplastic algorithm was used to solve non-linear equations. A homogenization technique based on elastoplastic behaviour of constituent materials has also been suggested by Canetta and Nova.[12,13]

In the following, the homogenization technique, which has been applied to the shear localization and rock joint analyses,[14] is modified to take into account of the volume fraction of inclusions, i.e., stone-columns. Both constituents are assumed to behave elastoplastically and a separate yield function for each constituent material is considered, i.e., *in situ* soil is represented

by the modified Cam-clay model, whereas the material of stone-columns is modelled by the Mohr–Coulomb criterion together with a non-associated flow rule. It is noted that the normal practice in elastoplastic analysis is to adopt an elastic predictor and plastic corrector scheme. However, if this procedure is followed, the corrected stress state may violate the equilibrium as well as compatibility conditions between the constituent materials of the composite which are the main ingredients of the homogenization technique. Here, a new sub-iteration scheme has been developed which satisfies these conditions fully.

An example of prediction of the behaviour of model circular footings on the stone-column reinforced foundations is presented. This shows good agreement with experimental observation. Finally, a new arrangement of stone-columns of variable length beneath a circular footing is studied with a view to economy in construction.

2. HOMOGENIZATION TECHNIQUE FOR MODELLING STONE-COLUMN REINFORCEMENT

In most cases, stone-columns are used to reduce settlement and increase bearing capacity of the *in situ* soil which supports foundations for storage tanks, buildings, etc. The pattern of stone-columns is uniform in most cases and, therefore, it is assumed that the stone-columns are scattered homogeneously and isotropically, i.e., uniformly, throughout the homogenization zone. It is also assumed that perfect bonding exists between *in situ* soil and stone-columns. Modelling of the elastoplastic behaviour of the foundations is performed by a using a separate yield function for each constituent and the equilibrium as well as the compatibility conditions are satisfied through stress/strain redistribution in successive iterations. In the following, a formulation for the axi-symmetric case is presented. This formulation can, of course, be modified for plane strain case such as applicable to the foundations of a long wall.

Following Pande *et al.*,[14] homogenization is carried out using the averaging rule as follows, see Figure 1:

$$\begin{aligned} \dot{\boldsymbol{\sigma}}^{\mathrm{eq}} &= \mu_i \dot{\boldsymbol{\sigma}}^i + \mu_j \dot{\boldsymbol{\sigma}}^j \\ \dot{\boldsymbol{\varepsilon}}^{\mathrm{eq}} &= \mu_i \dot{\boldsymbol{\varepsilon}}^i + \mu_j \dot{\boldsymbol{\varepsilon}}^j \end{aligned} \tag{1}$$

where, μ is an area (or volume) fraction, and includes eq, i and j represent homogenized equivalent material, *in situ* soil and stone-column, respectively. Homogenization is performed in a local co-ordinate system and the stress/strain relationships of each constituent are in the incremental form. In the above equation, the relevant components of stress/strain for the axisymmetric case are

$$\begin{aligned} \dot{\boldsymbol{\sigma}} &= \{\dot{\sigma}_r,\ \dot{\sigma}_z,\ \dot{\sigma}_{rz},\ \dot{\sigma}_\theta\}^{\mathrm{T}} \\ \dot{\boldsymbol{\varepsilon}} &= \{\dot{\varepsilon}_r,\ \dot{\varepsilon}_z,\ \dot{\varepsilon}_{rz},\ \dot{\varepsilon}_\theta\}^{\mathrm{T}} \end{aligned} \tag{2}$$

The equilibrium conditions between two constituents along the interface can be written in the local co-ordinate system as follows:

$$\begin{aligned} \dot{\sigma}_z^{\mathrm{eq}} &= \dot{\sigma}_z^i = \dot{\sigma}_z^j \\ \dot{\tau}_{rz}^{\mathrm{eq}} &= \dot{\tau}_{rz}^i = \dot{\tau}_{rz}^j \end{aligned} \tag{3}$$

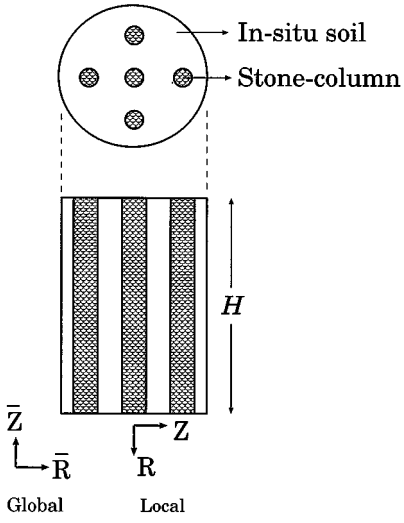

Figure 1. Homogenisation of stone-column with *in situ* soil

The kinematic conditions due to the assumption of bonding between the *in situ* and stone-columns are:

$$\begin{aligned} \dot{\varepsilon}_r^{\mathrm{eq}} &= \dot{\varepsilon}_r^i = \dot{\varepsilon}_r^j \\ \dot{\varepsilon}_\theta^{\mathrm{eq}} &= \dot{\varepsilon}_\theta^i = \dot{\varepsilon}_\theta^j \end{aligned} \tag{4}$$

and the constitutive equations for each constituent are described as

$$\begin{aligned} \dot{\boldsymbol{\sigma}}^i &= [D^i]\dot{\boldsymbol{\varepsilon}}^i \\ \dot{\boldsymbol{\sigma}}^j &= [D^j]\dot{\boldsymbol{\varepsilon}}^j \end{aligned} \tag{5}$$

where, $[D^i]$ and $[D^j]$ represent appropriate elastic of elastoplastic constitutive matrices of the two constituents in the local co-ordinate system.

Upon substituting equations (5) and (4) into equation (3):

$$D_{21}^i\dot{\varepsilon}_r^i + D_{22}^i\dot{\varepsilon}_z^i + D_{23}^i\dot{\gamma}_{rz}^i + D_{24}^i\dot{\varepsilon}_\theta^i = D_{21}^j\dot{\varepsilon}_r^j + D_{22}^j\dot{\varepsilon}_z^j + D_{23}^j\dot{\gamma}_{rz}^j + D_{24}^j\dot{\varepsilon}_\theta^j \tag{6}$$

$$D_{31}^i\dot{\varepsilon}_r^i + D_{32}^i\dot{\varepsilon}_z^i + D_{33}^i\dot{\gamma}_{rz}^i + D_{34}^i\dot{\varepsilon}_\theta^i = D_{31}^j\dot{\varepsilon}_r^j + D_{32}^j\dot{\varepsilon}_z^j + D_{33}^j\dot{\gamma}_{rz}^j + D_{34}^j\dot{\varepsilon}_\theta^j \tag{7}$$

or in view of equation (1)

$$\begin{aligned} \left(D_{22}^i + \frac{\mu_i}{\mu_j}D_{22}^j\right)\dot{\varepsilon}_z^i = {} & (D_{21}^j - D_{21}^i)\dot{\varepsilon}_r^{\mathrm{eq}} + \frac{D_{22}^j}{\mu_j}\dot{\varepsilon}_z^{\mathrm{eq}} - \frac{D_{23}^i}{\mu_i}\dot{\gamma}_{rz}^{\mathrm{eq}} \\ & + (D_{24}^j - D_{24}^i)\dot{\varepsilon}_\theta^{\mathrm{eq}} + \left(D_{23}^j + \frac{\mu_j}{\mu_i}D_{23}^i\right)\dot{\gamma}_{rz}^j \end{aligned} \tag{8}$$

$$\left(D^i_{33}+\frac{\mu_i}{\mu_j}D^j_{33}\right)\dot{\gamma}^i_{rz}=(D^j_{31}-D^i_{31})\,\dot{\varepsilon}^{eq}_r-\frac{D^i_{32}}{\mu_i}\dot{\varepsilon}^{eq}_z+\frac{D^j_{33}}{\mu_j}\dot{\gamma}^{eq}_{rz}$$
$$+(D^j_{34}-D^i_{34})\,\dot{\varepsilon}^{eq}_\theta+\left(D^j_{32}+\frac{\mu_j}{\mu_i}D^i_{32}\right)\dot{\varepsilon}^j_z \tag{9}$$

Arranging equations (8) and(9), the following equations for *in situ* soil are obtained:

$$[\delta]\dot{\boldsymbol{\varepsilon}}^i=[\alpha^i]\dot{\boldsymbol{\varepsilon}}^{eq}+[\beta^i][\delta]\dot{\boldsymbol{\varepsilon}}^j \tag{10}$$

where

$$[\delta]=\begin{bmatrix}0&1&0&0\\0&0&1&0\end{bmatrix}$$

$$[\alpha^i]=\begin{bmatrix}\dfrac{D^j_{21}-D^i_{21}}{C_1}&\dfrac{D^j_{22}}{\mu_jC_1}&\dfrac{-D^i_{23}}{\mu_iC_1}&\dfrac{D^j_{24}-D^i_{24}}{C_1}\\[2ex]\dfrac{D^j_{31}-D^i_{31}}{C_2}&\dfrac{-D^i_{32}}{\mu_iC_2}&\dfrac{D^j_{33}}{\mu_jC_2}&\dfrac{D^j_{34}-D^i_{34}}{C_2}\end{bmatrix}$$

$$[\beta^i]=\begin{bmatrix}0&\dfrac{D^j_{23}+\dfrac{\mu_j}{\mu_i}D^i_{23}}{C_1}\\[2ex]\dfrac{D^j_{32}+\dfrac{\mu_j}{\mu_i}D^i_{32}}{C_2}&0\end{bmatrix} \tag{11}$$

$$C_1=D^i_{22}+\frac{\mu_i}{\mu_j}D^j_{22}$$

$$C_2=D^i_{33}+\frac{\mu_i}{\mu_j}D^j_{33}$$

and for stone-columns,

$$[\delta]\dot{\boldsymbol{\varepsilon}}^j=[\alpha^j]\dot{\boldsymbol{\varepsilon}}^{eq}+[\beta^j][\delta]\dot{\boldsymbol{\varepsilon}}^i \tag{12}$$

and the coefficients of equation (12) can be similarly defined as in equation (11). It is noted that, because of symmetry in the elastic coefficients within the elastic limit, the above equation can be simplified to

$$\begin{aligned}[\delta]\dot{\boldsymbol{\varepsilon}}^i&=[\alpha^i]\dot{\boldsymbol{\varepsilon}}^{eq}\\[\delta]\dot{\boldsymbol{\varepsilon}}^j&=[\alpha^j]\dot{\boldsymbol{\varepsilon}}^{eq}\end{aligned} \tag{13}$$

or

$$\dot{\boldsymbol{\varepsilon}}^i = [\alpha_E^i]\dot{\boldsymbol{\varepsilon}}^{\mathrm{eq}}$$
$$\dot{\boldsymbol{\varepsilon}}^j = [\alpha_E^j]\dot{\boldsymbol{\varepsilon}}^{\mathrm{eq}} \tag{14}$$

where

$$[\alpha_E^i] = \begin{bmatrix} 1 & 0 & 0 & 0 \\ \dfrac{D_{21}^j - D_{21}^i}{C_1} & \dfrac{D_{22}^j}{\mu_j C_1} & \dfrac{-D_{23}^i}{\mu_i C_1} & \dfrac{D_{24}^j - D_{24}^i}{C_1} \\ \dfrac{D_{31}^j - D_{31}^i}{C_2} & \dfrac{-D_{32}^i}{\mu_i C_2} & \dfrac{-D_{33}^j}{\mu_j C_2} & \dfrac{D_{34}^j - D_{34}^i}{C_2} \\ 0 & 0 & 0 & 1 \end{bmatrix} \tag{15}$$

$$[\alpha_E^j] = \begin{bmatrix} 1 & 0 & 0 & 0 \\ \dfrac{D_{21}^i - D_{21}^j}{C_3} & \dfrac{D_{22}^i}{\mu_i C_3} & \dfrac{-D_{23}^j}{\mu_j C_3} & \dfrac{D_{24}^i - D_{24}^j}{C_3} \\ \dfrac{D_{31}^i - D_{31}^j}{C_4} & \dfrac{-D_{32}^j}{\mu_j C_4} & \dfrac{D_{33}^i}{\mu_i C_4} & \dfrac{D_{34}^i - D_{34}^j}{C_4} \\ 0 & 0 & 0 & 1 \end{bmatrix}$$

$$C_3 = D_{22}^j + \frac{\mu_j}{\mu_i} D_{22}^i$$

$$C_4 = D_{33}^j + \frac{\mu_j}{\mu_i} D_{33}^i$$

and equation (14) represents the structural relationship between component and homogenized medium within the elastic range. It is further noted that since

$$[D] = \frac{E}{(1+\nu)\ (1-2\nu)} \begin{bmatrix} (1-\nu) & \nu & 0 & \nu \\ \nu & (1-\nu) & 0 & \nu \\ 0 & 0 & \dfrac{(1-2\nu)}{2} & 0 \\ \nu & \nu & 0 & (1-\nu) \end{bmatrix} \tag{16}$$

for linear elastic materials in which E and v are the elastic modulus and Poisson's ratio, respectively, equation (15) can be simplified to

$$[\alpha_E^i] = \begin{bmatrix} 1 & 0 & 0 & 0 \\ \dfrac{D_{21}^j - D_{21}^i}{C_1} & \dfrac{D_{22}^j}{\mu_j C_1} & 0 & \dfrac{D_{24}^j - D_{24}^i}{C_1} \\ 0 & 0 & \dfrac{D_{33}^j}{\mu_j C_2} & 0 \\ 0 & 0 & 0 & 1 \end{bmatrix}$$

$$[\alpha_E^j] = \begin{bmatrix} 1 & 0 & 0 & 0 \\ \dfrac{D_{21}^i - D_{21}^j}{C_3} & \dfrac{D_{22}^i}{\mu_i C_3} & 0 & \dfrac{D_{24}^i - D_{24}^j}{C_3} \\ 0 & 0 & \dfrac{D_{33}^i}{\mu_i C_4} & 0 \\ 0 & 0 & 0 & 1 \end{bmatrix} \tag{17}$$

In the elastoplastic range, the following structural relationships can be established by substituting equation (12) into equation (10);

$$\begin{aligned} [\delta]\dot{\boldsymbol{\varepsilon}}^i &= ([I] - [\beta^i][\beta^j])^{-1}([\alpha^i] + [\beta^i][\alpha^j])\dot{\boldsymbol{\varepsilon}}^{\mathrm{eq}} \\ &= [S^i]\dot{\boldsymbol{\varepsilon}}^{\mathrm{eq}} \end{aligned} \tag{18}$$

or

$$\dot{\boldsymbol{\varepsilon}}^i = [S_1^i]\dot{\boldsymbol{\varepsilon}}^{\mathrm{eq}} \tag{19}$$

where $[I]$ is a 2×2 unit matrix and

$$[S^i] = ([I] - [\beta^i][\beta^j])^{-1}([\alpha^i] + [\beta^i][\alpha^j])$$

$$[S_1^i] = \begin{bmatrix} 1 & 0 & 0 & 0 \\ S_{11}^i & S_{12}^i & S_{13}^i & S_{14}^i \\ S_{21}^i & S_{22}^i & S_{23}^i & S_{24}^i \\ 0 & 0 & 0 & 1 \end{bmatrix} \tag{20}$$

Likewise

$$[\delta]\dot{\boldsymbol{\varepsilon}}^j = [S^j]\dot{\boldsymbol{\varepsilon}}^{\mathrm{eq}} \tag{21}$$

or

$$\dot{\boldsymbol{\varepsilon}}^j = [S_1^j]\dot{\boldsymbol{\varepsilon}}^{\mathrm{eq}} \tag{22}$$

where

$$[S^j] = ([I] - [\beta^j][\beta^i])^{-1}([\alpha^j] + [\beta^j][\alpha^i]) \tag{23}$$

$$[S_1^j] = \begin{bmatrix} 1 & 0 & 0 & 0 \\ S_{11}^j & S_{12}^j & S_{13}^j & S_{14}^j \\ S_{21}^j & S_{22}^j & S_{23}^j & S_{24}^j \\ 0 & 0 & 0 & 1 \end{bmatrix}$$

From equation (1), the following stress/strain relationship for homogenized equivalent material can be derived as

$$\begin{aligned} \dot{\boldsymbol{\sigma}}^{\mathrm{eq}} &= \mu_i \dot{\boldsymbol{\sigma}}^i + \mu_j \dot{\boldsymbol{\sigma}}^j = \mu_i [D^i][S_1^i]\,\dot{\boldsymbol{\varepsilon}}^{\mathrm{eq}} + \mu_j [D^j][S_1^j]\,\dot{\boldsymbol{\varepsilon}}^{\mathrm{eq}} \\ &= [D^{\mathrm{eq}}]\,\dot{\boldsymbol{\varepsilon}}^{\mathrm{eq}} \end{aligned} \tag{24}$$

where

$$[D^{\mathrm{eq}}] = \mu_i [D^i][S_1^i] + \mu_j [D^j][S_1^j] \tag{25}$$

or in global co-ordinate system,

$$\begin{aligned} \bar{\dot{\boldsymbol{\sigma}}}^{\mathrm{eq}} &= [T]^{-1}[D^{\mathrm{eq}}][T_1]\,\bar{\dot{\boldsymbol{\varepsilon}}}^{\mathrm{eq}} \\ &= [\bar{D}^{\mathrm{eq}}]\,\bar{\dot{\boldsymbol{\varepsilon}}}^{\mathrm{eq}} \end{aligned} \tag{26}$$

where

$$[\bar{D}^{\mathrm{eq}}] = [T]^{-1}(\mu_i [D^i][S_1^i] + \mu_j [D^j][S_1^j])\,[T_1] \tag{27}$$

and $[T]$ and $[T_1]$ are the appropriate transformation matrices. Equation (26) defines the constitutive relationship between homogenized equivalent stress and homogenized equivalent strain.

3. SOLUTION STRATEGY

With the formulation of the $\overline{D}^{\mathrm{eq}}$ matrix given in equation (27), standard finite element programs can be modified to solve the non-linear system of incremental stiffness equations in a number of ways. For instance, solution can be obtained if infinitesimally small load increments are used and stresses are updated based on the previous loading information. However, this method, known as the explicit forward Euler stress integration scheme, is unsatisfactory since the solution would eventually drift if finite load increments are used. To avoid this, various solution techniques in which finite load increments are used but iterations involving correction of the right-hand side of the system of non-linear equations to account for the stresses outside the yield surface are performed, e.g., the sub-incremental scheme with back projection along the effective stress direction,[15] and various numerical schemes can be found in Potts and Gens[16] or Sloan and Booker.[17] On the other hand, the implicit backward Euler stress integration scheme based on a Taylor series expansion of the current yield function satisfies the incremental consistency

condition and is known as stable, see Reference 18. Here, this scheme which yields more accurate results is used for both constituent materials though it takes more CPU time, see Reference 19. Details of the implicit backward scheme are not given here and can be found in Ortiz and Popov[18] and Alawaji *et al.*[19]

It is possible to devise several numerical schemes which would satisfy the equilibrium as well as kinematic conditions when stress states of one or both constituent materials are beyond the elastic limits. In this study, a sub-iteration scheme which makes successive corrections to restore the continuity of relevant stress/strain components is adopted. Here, incremental plastic strain of a constituent which undergoes elastoplastic deformation is directly added to the other constituent in the form of an incremental elastic strain, to satisfy the kinematic condition shown in equation (4). The distribution of the stress differences which violate the equilibrium condition can be carried out in a number of ways. The following are the possible schemes:

1. Add the stress difference to the stresses in *in situ* soil.
2. Add the stress difference to the stresses in stone-column.
3. Add the stress difference according to inverse proportion of the volume fractions.
4. Add half of the stress difference to the stresses in both constituents.

All the above schemes were tried but schemes 1, 3 and 4 showed divergence in many cases because the volume ratio of the *in situ* soil to stone-column is normally more than 3 and a large amount of residual forces are generated and accumulated. Scheme 2 is, therefore, used in this study. It is noted that the redistribution of stress differences only to the stone-columns may be controversial. However, adjustment of stresses in the *in situ* soil is also carried out through the global equilibrium iterations due to the residual forces calculated from the modified stone-column stresses. Figure 2 shows the sub-iteration scheme implemented in the current study. In Figure 2, superscripts i, j and eq denote the *in situ* soil, stone-column and equivalent material, respectively, and subscript n is the load (time) step. Furthermore, $[K^{\mathrm{eq}}]$ and $[B]$ represent the system stiffness matrix and the strain–displacement relationship, while $\mathrm{d}P$ and $\mathrm{d}\delta$ are the load increment and the corresponding displacement increment. Also $[S_1^i]$, $[S_1^j]$ and $[T_1]$ are introduced in equation (20), (23) and (27), respectively. Finally, F^i and F^j denote the yield functions of *in situ* soil and stone-column, respectively. Initially, return mappings based on the implicit backward Euler stress integration scheme are employed for both *in situ* soil and for stone-columns. The stress differences in z and rz components are next added to stone-column material and another return mapping is performed in stone-columns. The sub-iteration scheme in stone-column material is continued until the equilibrium condition is satisfied within prescribed tolerance. As implied in Figure 2, a tangential stiffness method is utilized throughout elastoplastic material behaviour. Although this solution method is expensive in terms of CPU times, a stable solution can be obtained compared with other solution techniques.

The constitutive models for each of the constituents of the stone-column reinforced foundation are discussed in the following section.

4. CONSTITUTIVE MODELS FOR CONSTITUENT MATERIALS

Elastoplastic behaviour of stone-column is modelled by Mohr–Coulomb yield criterion employing a non-associated flow rule. The non-associated flow rule in this case has a significant meaning in the sense that the *dilation* of the stone-column on shearing can be represented by adjusting the

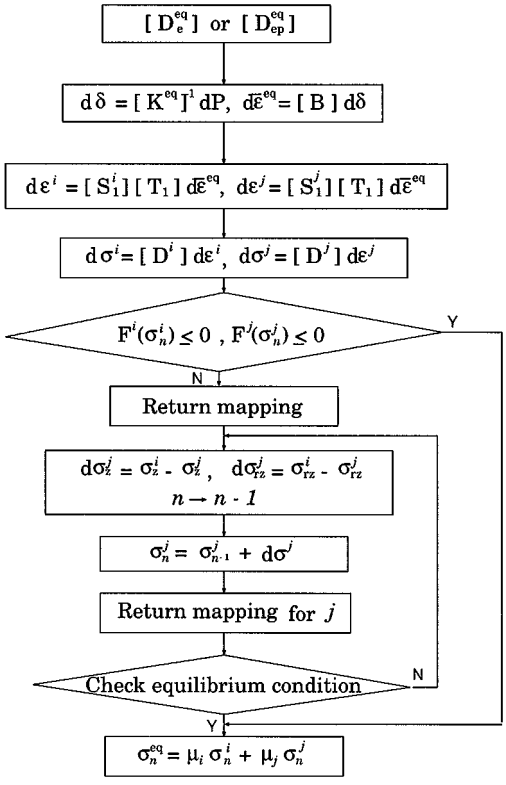

Figure 2. A sub-iteration scheme to correct the equilibrium condition

dilatancy angle. Meanwhile, to avoid possible numerical difficulties, a very small amount of linear hardening modulus is introduced in the model.

The non-linear behaviour of *in situ* soil is represented by the modified critical state model,[20] together with a tension cut-off. Therefore, as soon as the principal stress of the *in situ* soil reaches the prescribed tensile strength, a tensile failure mode rather than critical state yielding is assumed. Details of the modified critical state model are not described here and can be found elsewhere, e.g., References 21 and 22.

5. NUMERICAL EXAMPLE: ANALYSIS OF MODEL STONE-COLUMN REINFORCED FOUNDATIONS

In this section, the behaviour of the stone-column reinforced foundations is investigated. The numerical result is compared with the experimental data available.[23]

In the example shown in Figure 3(a), a model circular steel footing rests on stone-column reinforced foundations where the stone-columns are installed by the replacement method having 30 per cent of volume (area) ratio. Figure 3(b) shows finite element mesh used in the analysis which consists of 137 eight-noded isoparametric elements. A 2 × 2 Gauss integration rule is employed.

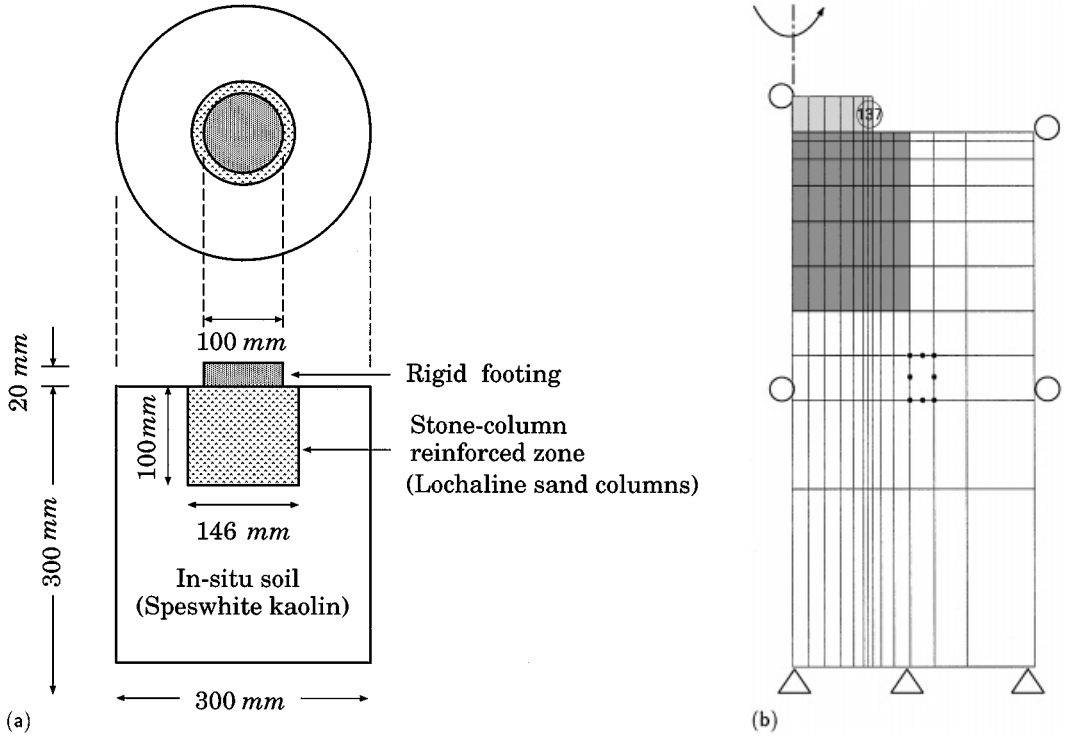

Figure 3. Geometry of stone-column reinforced foundation (a) geometry; (b) axi-symmetric finite element mesh

The experimental setup consists of a rigid footing made of a 20 mm thick, 100 mm diameter steel plate to which prescribed displacements are applied. The *in situ* soil is confined by a 300 mm diameter circular tank which is 300 mm deep. Stone-columns of 17·5 mm diameter are installed to a depth of 100 mm. A square pattern layout which consists of 5 × 5 grid of columns is used in the experiment. For full details of the experimental work, see References 23.

In the experiment, Speswhite kaolin clay is used for *in situ* soil and Lochaline sand for stone-columns. The following material characteristics of the Speswhite kaolin clay are estimated and the remaining parameters are obtained from A1-Tabbaa.[24]

(1) *Initial size of yield locus* $2p_{co}$: From Roscoe and Burland,[20]

$$\frac{p'}{2p_{co}} = \frac{M_{cs}^2 p'^2}{M_{cs}^2 p'^2 + q^2} \tag{28}$$

where $p' = (\sigma'_1 + 2\sigma'_3)/3$, $q = \sigma'_1 - \sigma'_3$ and σ'_1, σ'_3 being the major and minor effective principal stresses in the triaxial test. Also, M_{cs} is the slope of critical state line in $q - p'$ space obtained form A1-Tabbaa.[24] The value of p_{co} is obtained by simulating the history of consolidation of the clay in the tank and subsequent unloading. Simulation using estimated p_{co} value, 39·7 kPa, fits well with experimental data on clay foundation without stone-columns. However, to take into account of the installation disturbances caused by the displacement method, this value will be reduced to half when stone-column reinforced

foundation is considered. In fact, the bearing capacity of stone-column reinforced foundation using unalleviated p_{co} value overestimates the experimental one at the ratio of near two.

(2) *Young's modulus of kaolin clay* E_i: Theoretically, Young's modulus can be obtained from bulk modulus of clay, K_i, which is a function of mean effective stress, p' ,

$$K_i = \frac{1+e}{\kappa} p' \tag{29}$$

and, therefore,

$$E_i = 3(1-2v_i)\, K_i \tag{30}$$

where e is the mean value of void ratio in the range of stresses expected. However, it is found that Young's modulus estimated from the above equation is too high compared to the experimental data on clay foundation and, therefore, the value corresponding to the initial slope of available load–settlement curve of clay foundation is adopted in the numerical simulations.

(3) *Slope of swelling line* κ: Usual choice of κ ranges from 0·023 to 0·028[24] when the overconsolidation ratio is less than 2 and Al-Tabbaa[24] proposed a linear variation of κ as a function of the overconsolidation ratio up to 6. In this numerical study, $\kappa = 0{\cdot}028$ is adopted.

The material parameters used for kaolin are summarized in Table I where the earth pressure coefficient, K_o, is assumed as 0·7 since it is known that the values of K_o computed from the consolidation history using the critical state model are on the lower side.

The material properties of Lochaline sand required for the numerical model include the Young's modulus E_j, Poisson's ratio v_i, internal friction angle ϕ_j and dilatancy angle ψ_j which will be used in a Mohr–Coulomb yield criterion. Unfortunately, proper experimental data for Lochaline sand are not available so far and, therefore, the parameters for Hostun sand adopted from Saada and Bianchini[25] are used in the following, see Table II. It is noted that the internal friction angle, ϕ_j, has been increased by 10 per cent to account for the effect of compaction.

Numerical computations are based on the implicit backward Euler integration scheme and, to facilitate convergence, a small amount of cohesion of the stone-column material, $C_j = 3\,\text{kPa}$, has

Table I. Material properties used for Speswhite kaolin clay

Young's modulus	E_i	2000 kPa
Poisson's ratio	v_i	0·3
Friction angle	ϕ_i	23°
Compressibility constant	χ	13·53
Slope of consolidation line	λ	0·187
Slope of swelling line	κ	0·028
Slope of critical state line	M_{cs}	0·898
Initial void ratio	e_0	1·15
Specific gravity	G_s	2·68
Tensile strength	σ_{it}	0·1 kPa
Preconsolidation pressure	$2p_{co}$	40 kPa

Table II. Material properties used for Lochaline sand (column)

Young's modulus	E_j	189,243 kPa
Poisson's ratio	v_i	0·3
Friction angle	ϕ_i	35°
Dilatancy angle	ψ_j	10°
Cohesion	C_j	3 kPa

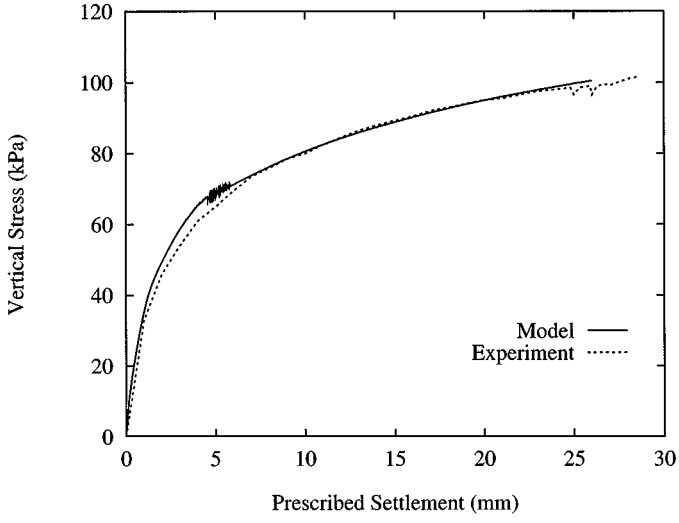

Figure 4. Prescribed settlement and vertical stress relationship

been used. Also, in addition to the prescribed incremental settlement on footing, a small amount of initial stresses in radial and hoop directions are applied. The initial stresses are assumed to be generated when installing stone-columns with the replacement method.

Drained analysis is performed to simulate physical experiment conducted by Stewart and Wu.[23] Figure 4 shows the relationship between prescribed footing settlement and the effective vertical stresses calculated underneath the footing. Also shown is the experimental data up to $\delta_o \approx 30{\cdot}0$ mm. The predicted vertical stress using homogenization technique is in good agreement with that of experiment. The numerical disturbance shortly after the onset of plastic straining is mainly due to the several tensile failures of the stone-columns at each load step.

Figure 5 illustrates the settlement pattern when the prescribed settlements, δ_o, are 1·0 and 10·0 mm. A punching effect due to stiff footing is clearly shown in Figure 5(b) and this causes tensile failures of the stone-columns as well as *in situ* soil. Also, the equilibrium iterations are rapidly increased as the tensile failure zone is enlarged. It is noted that, soon after the prescribed displacement is applied, the stone-columns fail first because stone-column material (sand) has a negligible cohesive strength compared to that of the clay. The bulging effect of stone-column is also clearly observed in the deformed pattern, Figure 5(b).

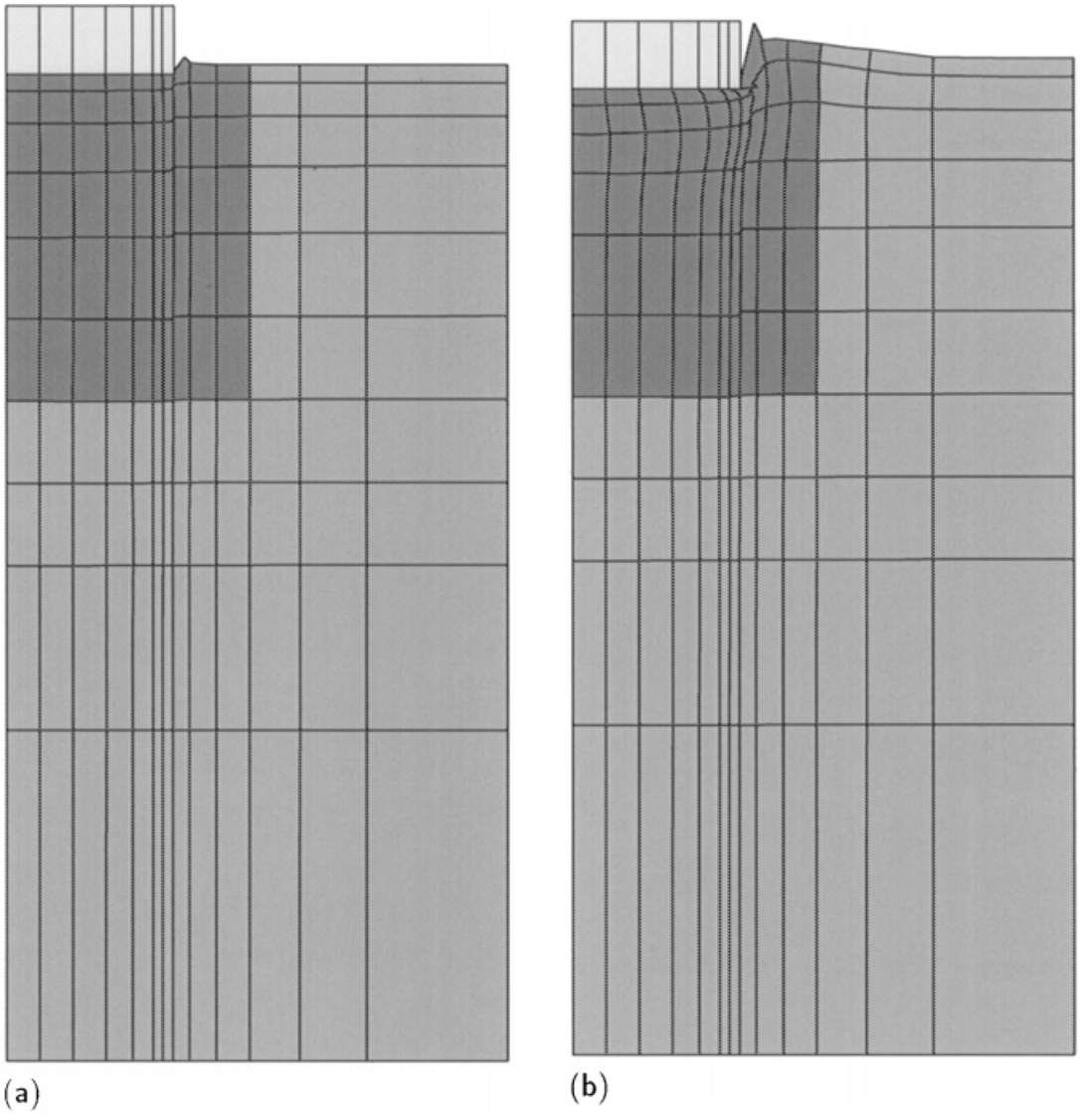

Figure 5. Deformation pattern (a) $\delta_0 = 1{\cdot}0\,\text{mm}$; (b) $\delta_0 = 10{\cdot}0\,\text{mm}$

The equilibrium conditions between *in situ* soil and stone-columns equation (3), are satisfied throughout elastic as well as elstoplastic range of the material behaviour. These could be visualized by contour plots of stress component of each constituent material and can be found in Lee.[26]

Variations of water content, w_c, in both constituents are next considered. The variations of water content can be correlated to the volumetric strains as follows:

The degree of saturation S_r for fully saturated soil is

$$S_r = \frac{w_c G_s}{e} = 1 \tag{31}$$

and the specific volume v is related to the void ratio as

$$v = 1 + e \tag{32}$$

Final volume of soil due to external loading is represented by

$$v_f = v_0 + \delta v = v_0(1 + \delta\varepsilon_v) \tag{33}$$

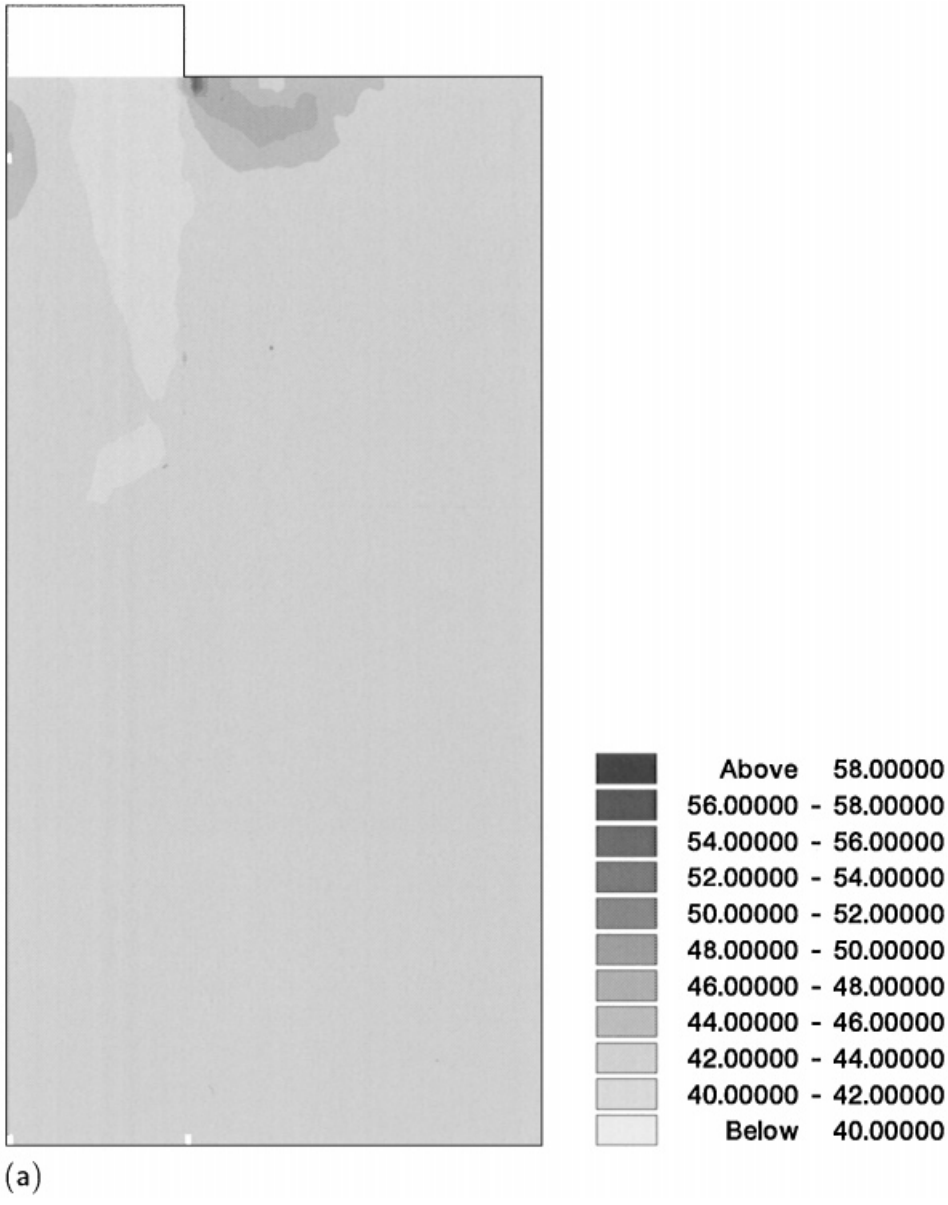

Figure 6. Variations of water content, $\delta_0 = 20{\cdot}0$ mm; (a) *in situ* soil; (b) stone-column

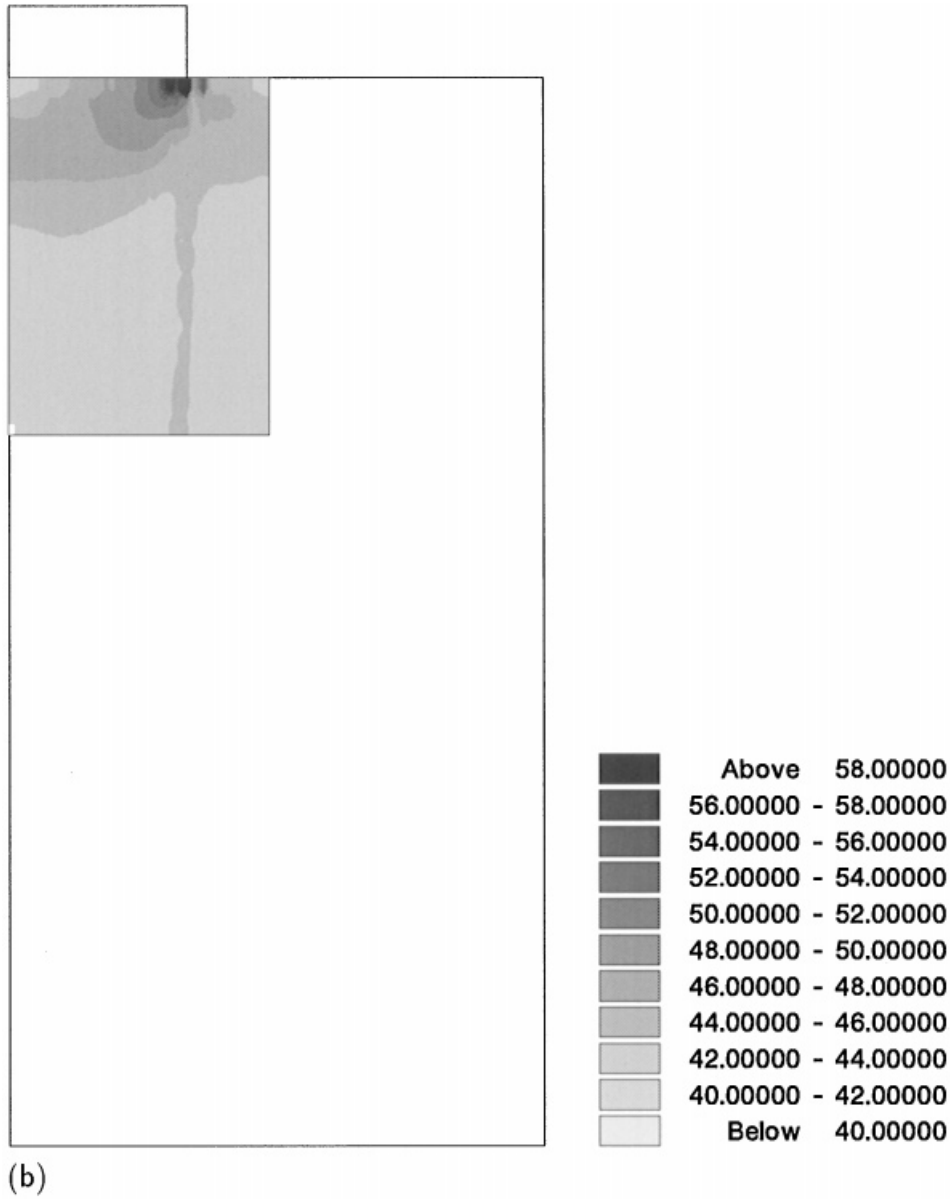

Figure 6. (Continued)

where, v_0, v_f and $\delta\varepsilon_v$ are the initial volume, final volume and change of volumetric strain, respectively. From equations (32) and (33),

$$e = v_0(1 + \delta\varepsilon_v) - 1 \tag{34}$$

Substituting this equation into equation (31),

$$\omega_c(\%) = \frac{(1 + e_o)\ (1 + \delta\varepsilon_v) - 1}{G_s} \times 100 \tag{35}$$

where, e_o is the initial void ratio. It is noted that the change of volumetric strain equation (33) can be obtained as follows:

$$\delta\varepsilon_v = \delta\varepsilon_v^e + \delta\varepsilon_v^p \tag{36}$$

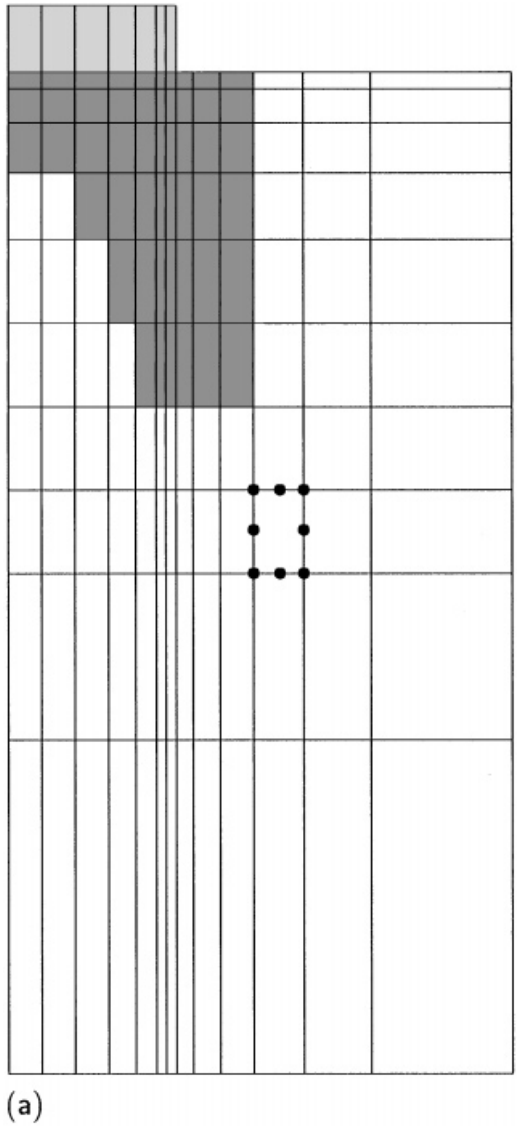

Figure 7. Analysis of foundation with reduced column length near the center (a) axi-symmetric finite element mesh; (b) prescribed settlement and vertical stress relationship

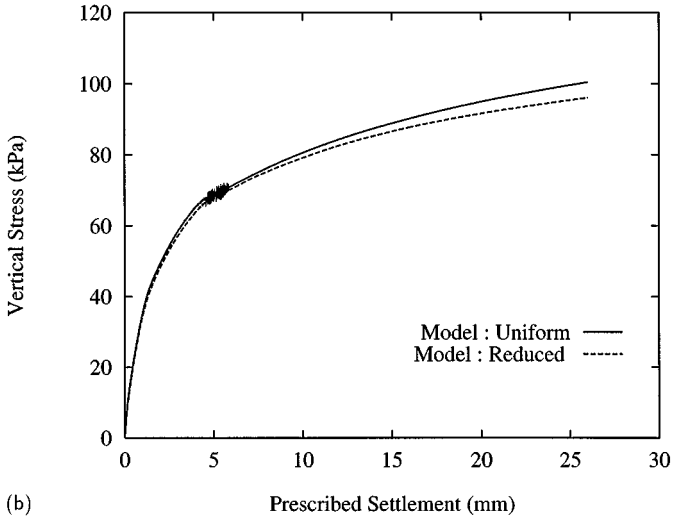

Figure 7. (Continued)

where elastic and plastic volumetric strains can be calculated from

$$\delta\varepsilon_{\mathrm{v}}^{\mathrm{e}} = \frac{\delta\sigma_{\mathrm{v}}}{K}$$

$$\delta\varepsilon_{\mathrm{v}}^{\mathrm{p}} = \delta(\varepsilon_r^{\mathrm{p}} + \varepsilon_z^{\mathrm{p}} + \varepsilon_\theta^{\mathrm{p}}) \tag{37}$$

If the values shown in Table I are used, the initial water content of *in situ* soil is computed as 43 per cent. Figure 6 illustrates the variations of water content in *in situ* soil and stone-columns. It is shown from the figure that the water in *in situ* soil is drained through stone-columns.

The distribution of vertical stresses for stone-columns is of special interest and it is noted that higher stresses are concentrated at the periphery of the steel footing. In view of this, a hypothesis that the effect of stone-columns may not perhaps be significant at the center of circular foundation. If this hypothesis is correct, it should be possible to reduce the lengths of stone-columns near the centre of the foundation without affecting significantly the bearing capacity or the settlement reduction factor. Figure 7(a) shows one of the finite element meshes in which a reduced zone of stone-column reinforcement in the centre of the foundation is considered. The finite elements involving equivalent material properties are reduced from 60 in Figure 3(b) to 49 in Figure 7(a). The load–settlement relationship for this case is shown in Figure 7(b). Also shown in the figure is the relationship when no reduction in the zone of homogenization is made (Figure 4). The bearing capacity as well as the settlements are not significantly different from each other regardless of the stone-column length in the middle of foundations.

6. CONCLUSIONS

A homogenization technique has been applied to the elastoplastic analysis of stone-column reinforced foundations. One of the main features of this study is the use of the equilibrium as well

as compatibility conditions throughout elastic and elastoplastic regime. For this, a sub-iteration scheme in which stress and strain jumps in various components in different constituents are systematically redistributed.

On the basis of the numerical studies considered here, the following conclusions are made:

(i) Using critical state model for *in situ* soil and using Mohr–Coulomb model for stone–columns, the elastoplastic analysis of stone–column reinforced foundations is performed and it is demonstrated the equilibrium as well as compatability conditions are always satisfied by using a sub-iteration scheme.
(ii) Implicit backward Euler integration scheme is implemented and proven to be stable compared to the explicit forward Euler integration scheme which is known to be unstable in many cases.
(iii) The prescribed settlement versus vertical stress curve shows that the numerical prediction is in good agreement with the vertical stresses measured underneath the rigid plate.
(iv) A scheme in which the length of stone-columns is variable near the centre of circular footing is proposed. This may lead to economy in construction without impairing the performance of circular stone–column reinforced foundations.

So far, two-dimensional prediction of the bearing capacity employing homogenization technique has been illustrated, however, it could be a good practice to perform a fully three-dimensional analysis of the reinforced foundations using conventional continuum elements in which stone–columns are modelled separately, and compare the results with the proposed model. The comparison as well as some parametric analyses in which the influence of spacing, diameter as well as length of columns are considered will be studied elsewhere.

ACKNOWLEDGEMENT

The research reported in the paper was financially supported by the Engineering and Physical Science Research Council (EPSRC) (formerly Science & Engineering Research Council, SERC). The experimental part of the work was carried out at the department of Civil Engineering, University of Glasgow under a separate grant also awarded by the EPSRC. The second author would like to acknowledge the opportunities to discuss the research reported here at several meetings provided by the EC grant ALERT-Geomaterials.

REFERENCES

1. G. A. Munfakh, L. W. Abramson, R. D. Barksdale and I. Juran, '*In situ* ground reinforcement', in *Proc. Symp. Soil Improvement—A Ten Year Update*, ASCE, New York, 1987, pp. 1–17.
2. J. M. O. Hughes and N. J. Withers, 'Reinforcing of soft cohesive soils with stone columns', *Ground Engng*., **7**(3)**,** 42–49 (1974).
3. V. Baumann and G. E. A. Bauer, 'The performance of foundations on various soils stabilized by the vibro-compaction method', *Can. Geotech. J*., **11,** 509–530 (1974).
4. R. R. Goughnour and A. A. Bayuk, 'Analysis of stone column – soil matrix interaction under vertical load', in *Proc. Int. Conf. Soil Reinforcements*, Paris, 1979, pp. 271–277.
5. H. Aboshi, E. Ichimoto, M. Enoki and K. Harada, 'The "compozer"—a method to improve characteristics of soft clays by inclusion of large diameter sand columns', in *Proc. Int. Conf. Soil Reinforcements*, Paris, 1979, pp. 211–216.
6. N. P. Balaam and J. R. Booker, 'Analysis of rigid rafts supported by granular piles', Int. J. Numer. Anal. Meth. Geomech., **5,** 379–403 (1981).
7. N. P. Balaam and J. R. Booker, 'Effects of stone column yield on settlement of rigid foundations in stabilized clay', *Int. J. Numer. Anal. Meth. Geomech*., **9,** 331–351 (1985).

8. J. K. Mitchell and T. R. Huber, 'Performance of a stone column foundation', *J. Geotech. Engng. ASCE*, **111,** 205–223 (1985).
9. H. F. Schweiger, 'Finite element analysis of stone column reinforced foundations', *PhD thesis*, Dept. Civil Eng., Univ. Coll. Swansea, U.K., 1989.
10. H. F. Schweiger and G. N. Pande, 'Numerical analysis of a road embankment constructed on soft clay stabilised with stone columns', in *Proc. Num. Meth. in Geomech.*, Innsbruck, 1988, pp. 1329–1333.
11. H. F. Schweiger and G. N. Pande, 'Modelling stone column reinforced soils—a modified Voigt approach', in *Proc. 3rd Numer. Models in Geomech.* (*NUMOG*), 1989, pp. 204–214.
12. G. Canetta and R. Nova, 'A numerical method for the analysis of ground improved by columnar inclusions', *Comput. Geotech.*, **7,** 99–114 (1989).
13. G. Canetta and R. Nova, 'Numerical modelling of a circular foundation over vibrofloted sand', in *Proc. 3rd Numer. Models in Geomech.* (*NUMOG*), 1989, pp. 215–222.
14. G. N. Pande, J. S. Lee and S. Pietruszczak, 'Homogenisation techniques for strain localisation and interface analysis', in *Proc. 2nd Asian–Pacific Conf. Comp. Mech.*, 1993, pp. 411–417.
15. D. R. J. Owen and E. Hinton, *Finite Elements in Plasticity*, Pineridge Press, Swansea, 1980.
16. D. M. Potts and A. Gens, 'A critical assessment of methods of correcting for drift from the yield surface in elasto-plastic finite element analysis', *Int. J. Numer. Anal. Meth. Geomech*, **9,** 149–159 (1985).
17. S. W. Sloan and J. R. Booker, 'Integration of Tresca and Mohr–Coulomb constitutive relations in plane strain elastoplasticity', *Int. J. Numer. Meth. Engng.*, **33,** 163–196 (1992).
18. M. Ortiz and E. P. Popov, 'Accuracy and stability of integration algorithm for elastoplastic constitutive relations', *Int. J. Numer. Meth. Engng.*, **21,** 1561–1576 (1985).
19. H. Alawaji, K. Runesson and S. Sture, 'Integration of constitutive equations in soil plasticity', *J. Engng. Mech. ASCE*, **117,** 1771–1790 (1991).
20. K. H. Roscoe and J. B. Burland, 'On the generalized stress-strain behaviour of 'wet' clay', in *Engineering Plasticity*, Cambridge University Press, Cambridge, 1968, pp. 535–609.
21. D. J. Naylor, G. N. Pande, B. Simpson and R. Tabb, *Finite Elements in Geotechnical Engineering*. Pineridge Press, Swansea, 1981.
22. D. M. Wood, *Soil Behaviour and Critical State Soil Mechanics*, Cambridge University Press, Cambridge, 1990.
23. B. Stewart and W. Hu, 'Analysis of regularly inhomogeneous soils: report on pilot tests', *Technical Report*, Dept. Civil Eng, University of Glasgow, U.K., May 1993.
24. A. Al-Tabbaa, 'Permeability and stress-strain response of speswhite kaolin, *Ph.D. thesis*, Dept. Civil Eng., University Cambridge, U.K., 1987.
25. A. Saada and G. Bianchini (eds), in *Proc. Constitutive Equations for Granular Non-cohesive Soils*, Balkema, 1988.
26. J. S. Lee, 'Finite element analysis of structured media', *Ph.D. thesis*, Dept. Civil Eng., University of Coll. Swansea, U.K., 1994.

